Geomechanics and Engineering, *Vol. 20, No. 1 (2020) 55-66*
DOI: https://doi.org/10.12989/gae.2020.20.1.055

Energy evolution characteristics of coal specimens with preformed holes under uniaxial compression

Na Wu[1a], Zhengzhao Liang[1], Jingren Zhou*[2] and Lizhou Zhang[3]

[1]State Key Laboratory of Coastal and Offshore Engineering, Dalian University of Technology, Dalian, 116024, China
[2]State Key Laboratory of Hydraulics and Mountain River Engineering, Sichuan University, No. 24 South Section 1, Yihuan Road, Chengdu 610065, China
[3]Chongqing Survey Institute, Chongqing, 401121, China

(Received October 14, 2019, Revised December 24, 2019, Accepted December 26, 2019)

Abstract. The damage or failure of coal rock is accompanied by energy accumulation, dissipation and release. It is crucial to study the energy evolution characteristics of coal rock for rock mechanics and mining engineering applications. In this paper, coal specimens sourced from the Xinhe mine located in the Jining mining area of China were initially subjected to uniaxial compression, and the micro-parameters of the two-dimensional particle flow code (PFC^{2D}) model were calibrated according to the experimental test results. Then, the PFC^{2D} model was used to subject the specimens to substantial uniaxial compression, and the energy evolution laws of coal specimens with various schemes were presented. Finally, the elastic energy storage ratio m was investigated for coal rock, which described the energy conversion in coal specimens with various arrangements of preformed holes. The arrangement of the preformed holes significantly influenced the characteristics of the crack initiation stress and energy in the prepeak stage, whereas the characteristics of the cumulative crack number, failure pattern and elastic strain energy during the loading process were similar. Additionally, the arrangement of the preformed holes altered the proportion of elastic strain energy $\boldsymbol{U_e}$ in the total energy in the prepeak stage, and the probability of rock bursts can be qualitatively predicted.

Keywords: coal specimen; preformed hole; particle flow code (PFC); energy accumulation; energy dissipation; eastic energy storage ratio

1. Introduction

The energy evolution of rock plays a significant role in accurately revealing the rock damage evolution, such as crack initiation, propagation, and coalescence (Bratov and Petrov 2007, Mu *et al.* 2019, Park *et al.* 2014, Steffler *et al.* 2003, Wasantha *et al.* 2014). Some investigations have shown that the crack initiation threshold (such as crack initiation stress and crack damage stress) is also closely related to the energy evolution of rock (Bruning *et al.* 2018, Sagasta *et al.* 2018, Zitto *et al.* 2015). Furthermore, the intrinsic reason for rock bursts is energy release (Bagde and Petroš 2009, José *et al.* 2007, Mark and Christopher 2016, Singh 1988). As an activity-induced geological hazard, rock bursts not only threaten the stability and safety of surrounding structures but also endanger the lives of nearby workers (Calleja and Nemcik 2016, Hebblewhite and Galvin 2017, Mark 2009, Fan and Liu 2019). To mitigate rock burst hazards, destressing techniques, such as drilling large diameter preformed holes and stress-relief blasting, have often been implemented to destroy the structural integrity of coal and reduce mining-induced energy accumulation (Nugroho and Purnama 2015, Wang *et al.* 2019). For the technique of drilling large diameter preformed holes, a number of holes were artificially drilled at varying distances in a roadway. Research on the energy accumulation and dissipation of coal specimens with preformed holes is of great significance for the mitigation of rock burst events through drilling large diameter holes.

Currently, numerous studies have been performed using different methods to study the failure mechanism of coal specimens with preformed holes. Theoretical analysis methods are often utilized based on elastic-plastic mechanics and damage mechanics (Gong *et al.* 2019, Jin *et al.* 2017, Kim *et al.* 2019). Many studies have employed theoretical analysis methods for understanding the failure mechanisms of rock masses with preformed holes. Laboratory testing is an important method for studying the failure mechanisms of rock masses. Lin *et al.* (2015) examined the influence of multiple holes on the peak strength of granite specimens under uniaxial compression. Fakhimi *et al.* (2002) performed a biaxial compression test on a sandstone specimen with a circular opening to simulate a loading-type failure around an underground excavation in brittle rock. Li *et al.* (2016) investigated the combined effects of stress concentration and crater-shaped pattern around the preformed holes under static and dynamic loading. Huang *et al.* (2019) studied the influence of bridge angle and number of preformed holes on the peak strength and peak strain of granite specimens contains multiple holes.

*Corresponding author, Ph.D.
E-mail: zhoujingrenscu@scu.edu.cn
[a]Ph.D. Student
E-mail: wndllgdx@126.com

ISSN: 2005-307X (Print), 2092-6219 (Online)

(a) Coal specimens

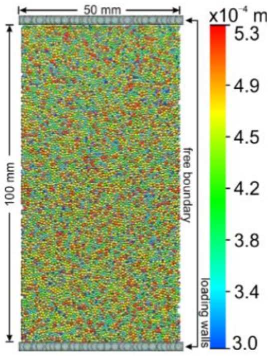

(b) Uniaxial compression setup

Fig. 1 Coal sample and PFC^{2D} model

Recently, an increasing number of studies have been performed using numerical simulation methods, such as the discrete element method, the finite element method and the extended finite element method. Cho *et al.* (2007) studied the damage development process of a rock mass with a preformed hole using a two-dimensional particle flow code (PFC^{2D}). Wong *et al.* (2006) used the material failure process analysis code to investigate the failure modes and strength characterization of brittle solids containing single pores with various pore diameters and sample widths. Sarfarazi al. (2018) investigate cracks initiations, propagations and coalescences of the concrete Brazilian discs containing a single cylindrical hole and or multiple holes. Zhang *et al.* (2011) simulated the damage process of marble specimens around a preformed hole and discussed the effect of the flaw on the failure mechanism of the rock mass. On this basis, they explored the mechanism of slabbing failure and rib spalling around the excavation boundary in deep high stress. Most researchers have focused on the macroscopic damage and micro-crack propagation in rock masses with artificial boreholes. However, the strain energy released in rock volume plays the pivotal role of abrupt structural failure of rock. (Steffler *et al.* 2003; Sujatha and Kishen 2003). Due to the experimental limitations, details of energy evolution could not always be comprehensively observed and assessed.

Boreholes are treated as efficient structures for distressing and reducing rock bursts. Stress distribution and the corresponding energy evolution law can be affected by borehole parameters and arrangements. This paper takes a viewpoint of energy evolution and failure mechanism of defective coal materials under uniaxial compression. A particle element model with calibrated microscopic parameters from a series of laboratory and numerical tests were adopted. The stored strain energy and dissipated energy under different artificial borehole parameters (diameter, spacing, relative angle and number of preformed holes) and preformed hole arrangements were studied. The concepts of the preformed hole area index K and the preformed hole vertical spacing index L were also proposed to analyze the influence of the variation in the preformed hole parameters on the energy evolution. These findings indicated that an optimized hole arrangement may have important consequences in terms of the rock bursts prevention during mining in deep coal seams.

2. Calibration of the micro-parameters in the PFC^{2D} model and establishment of the model

PFC^{2D} provided a numerical method that can qualitatively reproduce the mechanical mechanisms and phenomena that occur in a rock mass (Hazzard *et al.* 2000). The micro mechanical parameters are required to characterize the mechanical properties of the particles and bonding for particle flow theory. The parameters are usually calibrated before the numerical simulation as the micro mechanical parameters cannot be measured directly using laboratory tests. A trial and error method was used to determine the micro mechanical parameters until the macro mechanical parameters of the numerical model agreed with the results of the laboratory tests.

2.1 Physical tests

In this work, coal samples from a deep coal roadway of the Xinhe mine located in the Jining mining area of China were prepared for laboratory tests. The coal samples were drilled from No.3 coal rock by coring drill with an elevation angle of 5° - 10°. The specimens were cut into standard cylinders with a height to diameter ratio of 2:1, a length of 100 mm and a diameter of 50 mm in accordance with the size of international rock test specimens, as shown in Fig. 1(a). A series of triaxial and uniaxial compression experiments were performed using an MTS815 digitally servo-controlled rock mechanics testing machine. The macro mechanical parameters of the coal samples were obtained.

2.2 Calibration of the micro parameters in the PFC^{2D} model

According to the size of the coal specimen, a corresponding numerical model was established for micro parameter calibration, as shown in Fig. 1(b). The particles (colored by radius) represent the bulk sample with a size of 50 mm × 100 mm. The radii satisfy a Gaussian distribution with an average value of 0.4149 mm. The two loading walls at the top and bottom, which are composed of rigid particles, are constrained with horizontal displacement and spin. The loading walls provide a strain-controlled condition with a constant axial strain rate of $\dot{\epsilon}_{yy}$ (2.0×10^{-5}/s is adopted in the tests). The lateral boundary condition is

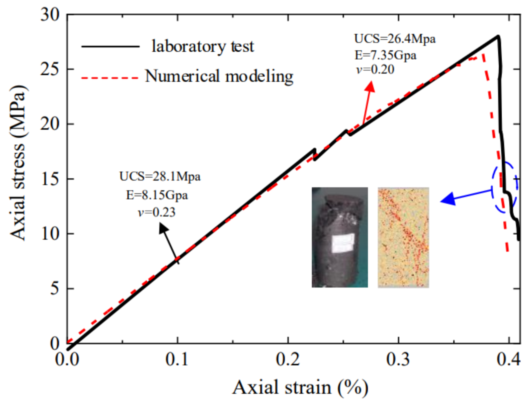

(a) Stress-strain curves of the coal specimens

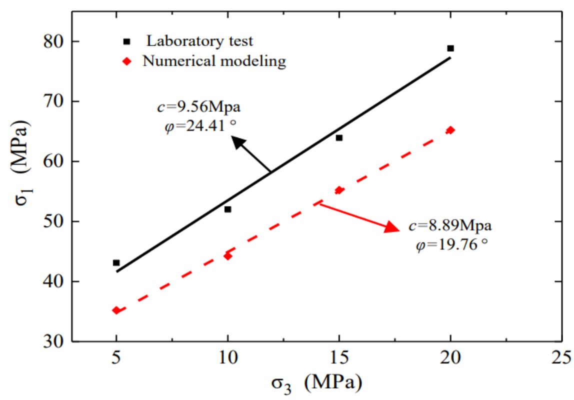

(b) Relationship between the peak strength and the confining pressure

Fig. 2 Comparison of the experimental and numerical results

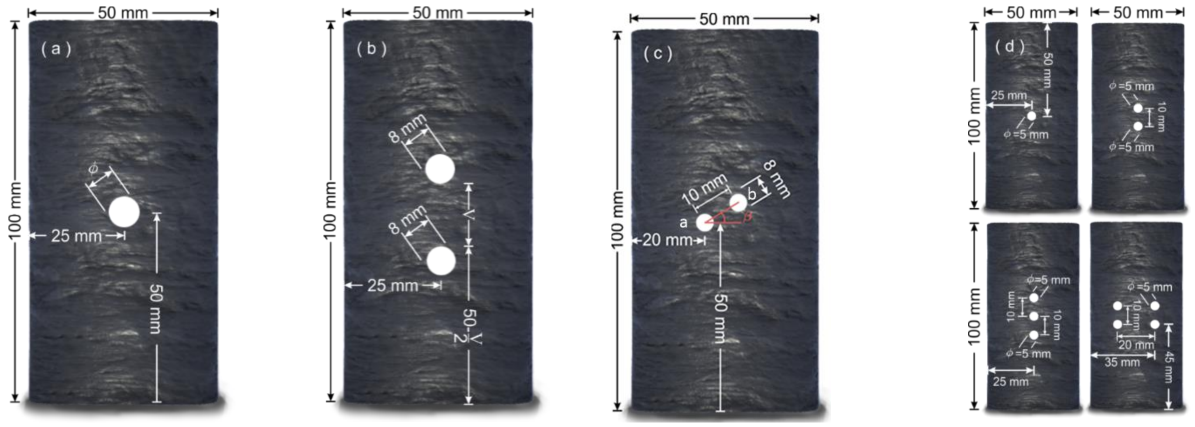

Fig. 3 Sketch of arrangements of preformed holes in coal specimens: (a) various artificial borehole diameters, (b) various vertical spacings, (c) various relative angles and (d) various artificial borehole numbers

Table 1 Micro mechanical parameters of coal specimens in numerical simulation

Micro mechanical parameter	Value	Micro mechanical parameter	Value
Density (kg·m^{-3})	1850	Parallel-bond modulus (GPa)	5.5
Average particle radius (mm)	0.4149	Parallel-bond stiffness ratio	2.0
Ratio of largest to smallest radius	1.766	Parallel-bond mean normal strength (MPa)	20
Particle-particle contact modulus (GPa)	5.5	Parallel-bond normal strength, standard deviation (MPa)	10
Particle stiffness ratio	2.0	Parallel-bond mean shear strength (MPa)	30
Particle friction coefficient	0.8	Parallel-bond shear strength, standard deviation (MPa)	10

Table 2 Comparison of experimental and numerical results

	UCS (MPa)	Poisson's ratio	Elastic modulus (GPa)	Cohesion (MPa)	Friction angle (°)
Experimental	28.1	0.23	7.60	9.56	24.41
Numerical	26.4	0.215	7.35	8.89	19.76
Error	6.24%	6.74%	3.34%	7.26%	21.05%

set to free. The two particles i and j, which have positions of $\boldsymbol{r}_i$ and $\boldsymbol{r}_j$, radii of R_i and R_j and rotations of θ_i and θ_j, respectively, are parallel-bonded when their overlap $\delta = R_i + R_j - \|\boldsymbol{r}_{ij}\|_2 > 0$, where $\boldsymbol{r}_{ij} = \boldsymbol{r}_i - \boldsymbol{r}_j$. The normal-force increment is calculated as $\Delta\bar{f}_n = \Delta f_n + k_n A \Delta\delta_n$, where $A = 2 \cdot \min(R_i, R_j)$, f_n is the linear normal spring force, and k_n is the bond normal stiffness. The tangential spring force increment$\Delta\bar{f}_s = \Delta f_s + k_s A \Delta\delta_s$, where f_s is the linear tangential spring force, k_s is the bond shear stiffness, and $\Delta\delta_{n(s)}$ is the relative normal-displacement (shear-displacement) increment between the two particles in contact. Note that $\Delta\delta_n$ is calculated as $\Delta\delta_n = v_n \cdot \Delta t$, where $v_n = \dot{\boldsymbol{r}}_{ij} \cdot \boldsymbol{e}_n$. Furthermore, $\Delta\delta_s$ is calculated as $\Delta\delta_s = v_s \cdot \Delta t$, where $v_s = \dot{\boldsymbol{r}}_{ij} \cdot \boldsymbol{e}_s + R_i\dot{\theta}_i + R_j\dot{\theta}_j$. In the 2D case, only rotations about the *z*-axis are allowed, and the other types of rotations, such as twisting-rotation and bending-rotation, are zeroed. Bond forces are removed when stresses, such as tension, shear, twisting and bending, exceed the corresponding bond strength. Then, particles interact with each other via linear springs, i.e., $\Delta\bar{f}_n = \Delta f_n$ and $\Delta\bar{f}_s = \Delta f_s$.

The micro-scale properties such as particle radius, stiffness, friction coefficient and bond strengths should be determined. A series of numerical tests were performed to reproduce the true uniaxial compression. The loading condition which is identical to the laboratory test was applied on the numerical specimen through two rigid boundary walls with a constant deformation rate. Strain and stress variations were recorded through wall displacement and resultant forces on walls, respectively. The resulting load curve $\sigma = \sigma_{yy}$ with $\sigma_{xx} = 0$ against shear strain $\epsilon = \epsilon_{yy}$ and the failure patterns at the postpeak stage are reported in Fig. 2. The uniaxial compressive strength (UCS) is 28.1 MPa and Young's modulus is about 8.15 GPa according to the experimental results. In the simulation, the UCS and Young's modulus is 26.4 MPa and 7.35 GPa, respectively. The simulation result is close to the measured response of experimental sample. The appropriate micro parameters of the coal are determined and shown in Table 1. The stress-strain curve declined quickly after reaching the peak strength, which indicated that the coal mechanical behavior was brittle under uniaxial compression. The failure pattern of the coal specimen was a combination of axial splitting and local shearing. The particles and the force chain are colored by stress magnitude and contact force. A stress tensor around a particle is calculated as $\sigma_{ij} = \frac{1}{V}\sum_n \boldsymbol{f}_{ij} \otimes \boldsymbol{l}_{ij}$, where V is the area of a given circular region centered at the corresponding circle that contains n internal contacts, $\boldsymbol{f}_{ij}$ is the contact reaction force and $\boldsymbol{l}_{ij}$ is the branch vector joining the center of the particles in a contact. The stress magnitude is calculated by $|\sigma| = \sigma{:}\sigma$. A comparison of the average mechanical parameters from the experimental and numerical results are given in Table 2. The minimum error of the corrected elastic modulus was 3.07%, whereas the maximum error of the corrected friction angle was 19.04%. This difference could be caused by micro structures and heterogeneity in coal specimen (Fan *et al.* 2017). The macro-mechanical parameters obtained from the numerical simulation were in good agreement with those from the experimental results.

2.3 Model establishment

According to the calibrated micro mechanical parameters, numerical models with dimensions of 50 mm × 100 mm were established. To explore the energy evolution law of coal under uniaxial compression, four types of simulation schemes were designed, as sketched in Fig. 3.

Scheme one: A preformed hole was located in the center of the model. The various diameters D of the preformed hole were set to 0 mm (intact coal specimen), 5 mm, 10 mm, 15 mm and 20 mm, as shown in Fig. 3(a).

Scheme two: The diameter of each preformed hole was set to 8 mm. The various vertical spacings V between two preformed holes were 0 mm (intact coal specimen), 5 mm, 10 mm, 15 mm, 20 mm and 25 mm, respectively, as shown in Fig. 3(b).

Scheme three: The diameters of the two preformed holes were both 5 mm, and their spacing was set to 10 mm. The locations of the two preformed holes are plotted in Fig. 3(c). The relative angles of the preformed holes βwere fixed at 0°, 30°, 60° and 90°. Preformed hole "a" is kept unchanged, and preformed hole "b" is rotated with the relative angle.

Scheme four: The diameter of each preformed hole was set to 5 mm. The vertical and horizontal spacings between preformed holes were 10 mm and 20 mm, respectively. The various numbers of preformed holes N were 0 (intact coal specimen), 1, 2, 3 and 4. A detailed description is given in Fig. 3(d).

3. Calculation and analysis of energy during coal deformation under uniaxial compression

It is widely known that the deformation and failure process of rock mass under uniaxial compression is an essentially process of energy conversion. The process can be resolved into four stages from the perspective of energy evolution: energy input, energy accumulation, energy dissipation and energy release (Cai *et al.* 2004). Assume that the rock sample does not exchange heat with the outside environment during the entire deformation and failure process of uniaxial compression, i.e., the rock sample is a closed system that is isolated from the outside world. According to the first law of thermodynamics, the equilibrium relationship between energy can be described as follows:

$$U_t = U_e + U_d \tag{1}$$

where U_t is the total accumulated work done by external force, U_e is the elastic strain energy stored in the coal body, and U_d is the dissipated energy during the inelastic deformation.

Coal is a special kind of rock material in which a unit volume of coal is approximately linearly elastic, homogeneous and isotropic. During the entire process of deformation and failure of a unit volume of coal, the materials are always accompanied by energy accumulation and dissipation. The coal is deformed by external action, and this deformation includes an elastic deformation stage and a plastic deformation stage. Fig. 4 shows the relationship between energy transformation and the stress-strain state of an ideal unit volume of coal. The total work U_t is the area under the stress-strain curve. The blue area in Fig. 4 is the elastic strain energy U_e, whereas the purple area is the dissipated energy U_d. In the process of rock failure, the elastic strain energy (U_e) gradually increases and develops from a stable state to an unstable state while storing internal energy. The greater the performance is, the more intense the energy release after rock failure and the higher the probability of dynamic failure. The dissipated energy (U_d) is related to the initiation, propagation and translocation of cracks in the rock. Therefore, the smaller the energy is in this part, the more likely the rock is to be destroyed and lose its strength and bearing capacity. However, this part of the energy does not directly affect the postpeak failure.

In the uniaxial compression test of the PFC^{2D} model, if a continuous force is applied on the model (the upper and

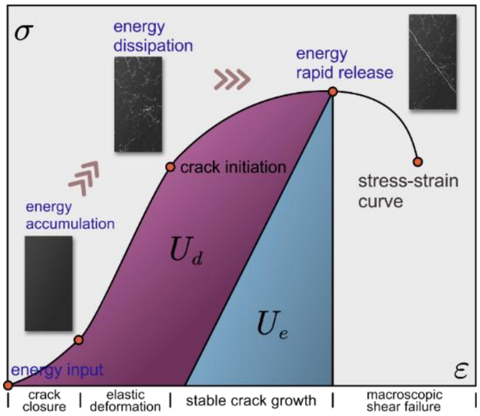

Fig. 4 Relationship between the energy transformation and the stress-strain state of a unit volume of coal

lower boundaries have only axial displacement and no angular displacement), the work E_w of the particle bond can be determined (Zhang *et al.* 2011). The work U done by the external force can be determined by the following equation:

$$U_t = E_{pre} + (F_1 \Delta U_1 + F_2 \Delta U_2) \tag{2}$$

where E_{pre} is the input energy at the end of time-step n, F_1 and F_2 are the forces of the two loading walls acting on particles at the end of time-step $n+1$, and ΔU_1 and ΔU_2 are the axial displacements of the walls at the end of time step $n+1$.

In the bonded particle model (BPM), the particles are bonded at the contacts. These bonds establish an elastic interaction between particles, and each parallel bond can be envisioned as a set of elastic springs with constant normal and shear stiffness (Zhang *et al.* 2011). Therefore, the total U_e can be resolved into the form of bond energy U_{pb} and stored contact strain energy U_c. In this paper, the energies U_e, U_{pb} and U_c are expressed by the following equation.

$$U_e = U_{pb} + U_c \tag{3}$$

$$U_{pb} = \frac{1}{2}\sum_{N_{pb}}\left(\frac{|\bar{F}_i{}^n|^2}{A\bar{K}^n} + \frac{|\bar{F}_i{}^s|^2}{A\bar{K}^s} + \frac{|\bar{M}_3|^2}{I\bar{K}_n}\right) \tag{4}$$

$$U_c = \frac{1}{2}\sum_{N_c}\left(\frac{|F_i{}^n|^2}{K^n} + \frac{|F_i{}^s|^2}{K^s}\right) \tag{5}$$

where N_{pb} is the number of parallel bonds; $\bar{F}_i{}^n$, $\bar{F}_i{}^s$ and $\bar{M}_3$ are the magnitudes of the normal and shear components and the bending-moment of the parallel bonds, respectively; $\bar{K}^n$ and $\bar{K}^s$ are the normal and shear stiffness of the parallel bonds, respectively; I is a constant calculated by $I = \frac{2}{3}R^3$ with $R = \min(R_i, R_j)$ in the 2D case; $A = 2R$ is the section area of the parallel bonds; N_c is the number of contacts; F_i^n and F_i^s are the magnitudes of the normal and shear components of the contact force, respectively; and K^n and K^s are the normal and shear contact stiffness, respectively.

The total work U_t, the bond energy U_{pb} and the stored contact strain energy U_c can be calculated with Eqs. (2) through (5). Then, the dissipated energy U_d can be obtained with Eq. (1).

4. Results and analysis

4.1 Characteristics of the crack initiation stress

Crack initiation stress is one of the three characteristic stresses in the progressive failure process of coal specimens, which is an important parameter reflecting the material properties of coal specimens. In this paper, the crack initiation stress is defined as the stress .corresponding to 1% of the number of cracks at the peak stress (Potyondy 2004). A Crack in PFC model is defined as the bond break between particles. Based on the numerical results, the crack initiation stress of the coal specimens in schemes one and two were investigated, as shown in Fig. 5.

Fig. 5(a) and Fig. 5(c) shows that the crack initiation stress and storage strain energy gradually decreased as the preformed hole diameter increased. When the hole diameter D is small (smaller than 5 mm), the dissipation energy in the initial stage is close to that in the intact coal (D = 0 m). The stored strain energy in this condition is relatively high and is dissipated mainly by driving the formation of the new fracture surface. It indicates that in the post-peak stage, the strain energy would releases rapidly, similar to the behaviour of an intact coal rock. When D increases from 10 mm to 15 mm, the crack iniation stress slightly decreases from 0.827 Mpa to 0.814 Mpa (reduced to 98.4%) while the storage strain energy markedly decreases from 217 kN·m to 143 kN·m (reduced to 65.9%). It means that the hole radius increment in this range (5 mm to 10 mm) would reduce the capability of strain energy storage and promote energy dissipation in the top and bottom part of the hole, but has limited effect on the time of coal entering yield. Energy dissipation in this stage is mainly caused by friction of fracture surface, which indicates that the coal is progressively broken. For larger hole diameter (diameter ranges from 15 to 20 mm), the energy before peak is more easily dissipated due to the lower crack initiation stress, which correspondingly improves the degree of failure of coal.

Fig. 5(b) indicates that the crack initiation stress first decreased and then remained approximately constant as the distance between the two preformed holes increased. The storage energy limit decreased as V ranges from 0 mm to 15 mm and then increased as V ranges from 15 mm to 25 mm (Fig. 5(d)). When the vertical distance is 5 mm, the crack initiation stress is similar to that of intact coal, but the storage energy is reduced to 178.41 kN m, with a decrease of 36.19%. The size of rock bridge between the two holes becomes a key factor to energy storage capacity. A small rock bridge is weak and could be easily damaged when subject to horizontal tensile stress. The rock bridge can simultaneously lead to obvious superimposition of stress near holes, crack gathering and triggers coal failure and drastic drop of strain energy. Storage strain energy decreases slowly to the limit when V is between 10 mm and 15 mm. When V increases to 20 mm and 25 mm, the

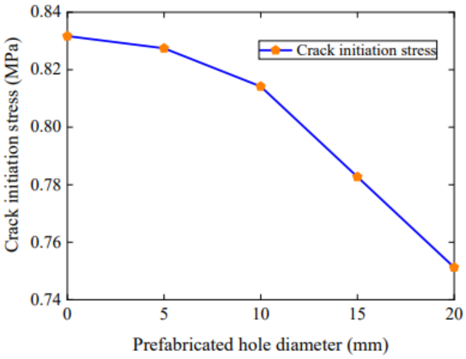

(a) Crack initiation stress with various diameters of artificial boreholes

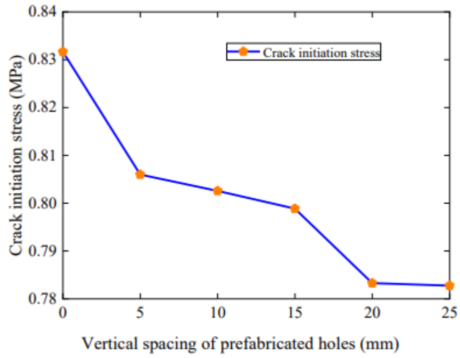

(b) Crack initiation stress with various vertical spacings of preformed holes

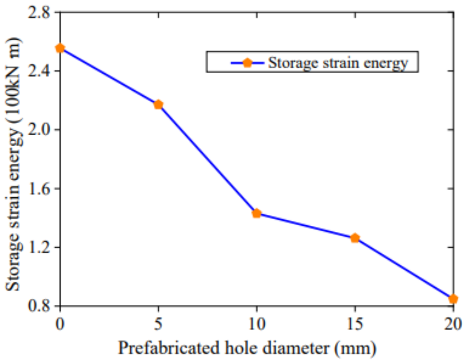

(c) Storage strain energy with various diameters of artificial boreholes

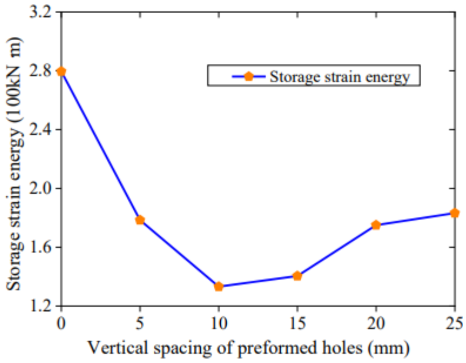

(d) Storage strain energy with various vertical spacings of preformed holes

Fig. 5 Crack initiation stresses and storage strain energy of the coal specimens in schemes one and two

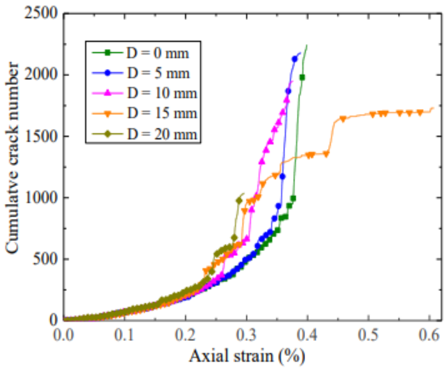

(a) Various diameters of preformed holes

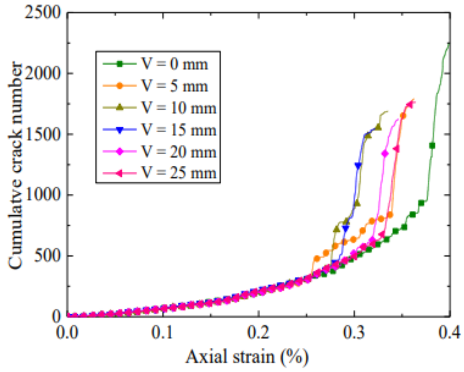

(b) Various vertical spacings of preformed holes

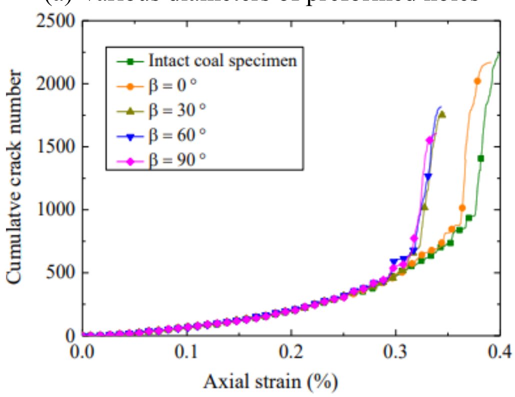

(c) Various relative angles of preformed holes

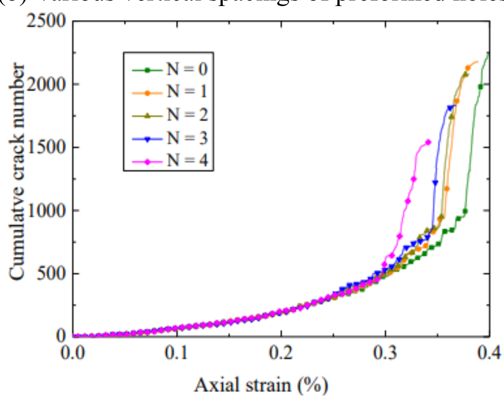

(d) Various numbers of preformed holes

Fig. 6 Cumulative crack number-axial strain curves of the coal specimens

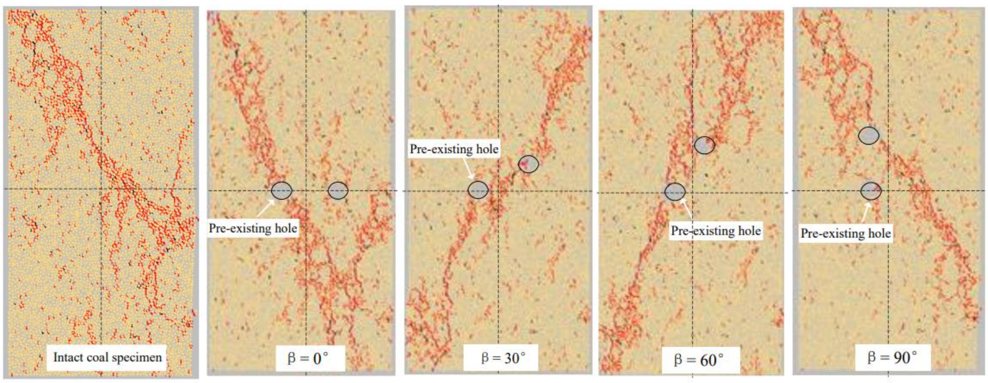

Fig. 7 Failure patterns of coal specimens containing preformed holes with different relative angles

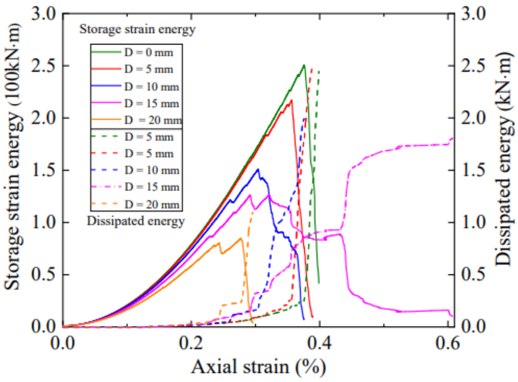

(a) Various diameters of preformed holes

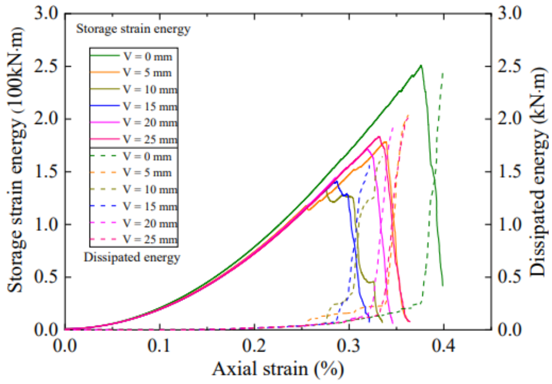

(b) Various vertical distances of preformed holes

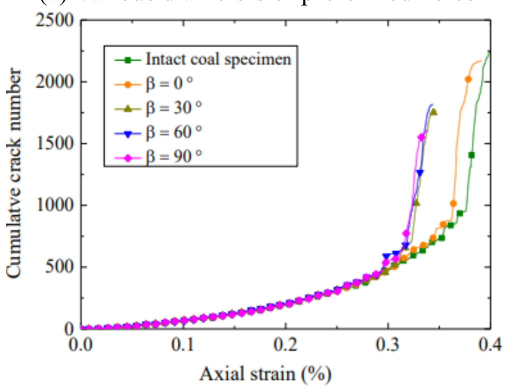

(c) Various relative angles of preformed holes

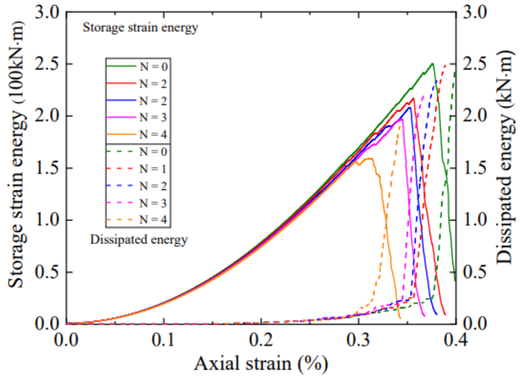

(d) Various numbers of preformed holes

Fig. 8 Dissipated energy and elastic strain energy of coal sample

incensement of rock bridge size weakened the interaction between holes. The rock bridge becomes relatively harder to be damaged and the cracks attempts to appear on the two sides of the bridge, which would prevent energy release. Then, the energy storage limit are relatively increased. Therefore, the distributions of the preformed holes have a significant influence on the variation law of the crack initiation stress.

4.2 Crack development characteristics

Dissipated energy is closely related to the initiation, propagation and translocation of cracks in the coal rock; therefore, the cumulative process of cracking in the coal specimens under uniaxial compression was analyzed. Fig. 6 shows the crack cumulative law during the loading process of the coal specimens. The crack cumulative laws of all specimens were similar (except the coal specimen containing a preformed hole with a 15 mm diameter) and can be divided into three stages: initiation stage, stable crack development stage and rapid crack development stage. In the initiation stage, no cracks occurred, and the cumulative crack number was approximately zero. In the second stage, the cumulative crack numbers developed slowly and steadily. The curves of the cumulative crack numbers were almost coincident in the first part and became discrete as the axial strain increased. As the loading increases further, the number of cumulative cracks linearly increased to the maximum value. This phenomenon occurred because the internal structure of the coal specimen was destroyed, and the macroscopic failure surface of the rock formed. For the coal specimen containing a preformed hole with a 15 mm diameter, the number of cumulative cracks first slowly developed, then quickly increased to the maximum value and finally remained approximately constant. The reason for this phenomenon was that this coal specimen may exhibit ductile failure, whereas the other specimen may exhibit brittle failure.

4.3 Characteristics of the failure patterns

The failure patterns of coal specimens containing preformed holes with different relative angles are shown in Fig. 7. The results showed that the relative angle would affect the level at which the axial loading stress acts on the rock bridge and the interaction between the preformed holes. The coal specimens containing preformed holes with different relative angles were damaged through a shear plane. However, the form of the distributions of the shear planes were distinct. For the intact coal specimen, the shear plane intersected the upper left diagonal and lower right side of the model. For the two preformed holes with a 0° relative angle, the shear plane just runs through the left preformed hole and is nearly distributed along the diagonal of the coal specimen. For the two preformed holes with 30° and 60° relative angles, the shear planes passed through a rock bridge between two openings and were distributed along the diagonal of the coal specimen. When the relative angle of the two preformed holes was 90°, the shear plane only ran through the upper preformed hole, and the distribution was similar to that of the intact coal specimen. In summary, the distributions of the through shear planes of the intact coal specimen and the specimen containing two preformed holes with a 90° relative angle were similar to each other and opposite to the distributions of the other specimens. Therefore, the relative angle of the preformed holes had little influence on the failure pattern but had an important influence on the distribution form of the shear planes of the coal specimen.

4.4 Characteristics of the dissipated energy and elastic strain energy during the loading process

Fig. 8 shows that elastic strain energy U_e and dissipated energy U_d in the coal specimens varied with respect to the axial strain. The change trends of the elastic strain energy U_e and dissipated energy U_d were similar to each other, except for the coal specimen containing a preformed hole with a 15 mm diameter. The change trends of the elastic strain energy U_e (or dissipated energy U_d) can also be divided into three stages: an initiation stage, a slow increasing stage and a rapid decreasing (increasing) stage. During the initiation stage, most of the energy was used for compaction of the intergranular pores, micro-fractures and elastic deformation in the coal specimen, and the input energy was stored in the coal specimens as elastic strain energy U_e. Therefore, the dissipated energy U_d was nearly zero in the initiation stage. Under the constant work, micro-cracks were constantly forming in the coal samples and expanding as the loading increased (as shown in Fig. 6). During this period, the total energy U absorbed by the coal specimen was converted into elastic strain energy U_e and dissipated energy U_d. Therefore, the elastic strain energy U_e and dissipated energy U_d nonlinearly increased with increasing axial strain. Additionally, the elastic strain energy U_e was much larger than the dissipated energy U_d, which indicated that most of the total energy U accumulated as elastic strain energy U_e in the form of elastic deformation and a proportion of the energy accumulated as dissipated energy U_d in the form of inelastic deformation. As the axial loading further increased, the elastic strain energy U_e increased to the energy storage limit (ESL) of the coal specimens. The elastic strain energy U_e plummeted and the dissipated energy U_d suddenly increased. This phenomenon occurred because the internal structure of the coal sample was destroyed, the micro-cracks connected to form a macroscopic failure surface, and the coal sample exhibited brittle damage. For the coal specimen containing a preformed hole with a 15 mm diameter, the elastic strain energy U_e first slowly increased to the ESL, then fluctuated and remained approximately constant after undergoing a rapid decrease; this coal specimen exhibited plastic behavior. The change trend of the dissipated energy U_d first slowly increased, then quickly increased to the maximum value and finally remained approximately constant, which is consistent with the development of the cumulative crack number. A comparison of Figs. 6 and 8 shows that the deformation and failure of the coal sample were the result of energy-driven instabilities, which included energy accumulation, dissipation and conversion (Munoz *et al.* 2016). Additionally, the change trends of the elastic strain energy U_e and dissipated energy U_d can reveal the elastic-brittle-plastic behavior.

4.5 Energy characteristics in the prepeak stage

Fig. 9 shows the energy evolution of the coal specimens. A comparison of the various schemes shows that the variation tendencies of total energy, elastic strain energy and dissipated energy of the coal specimens had both similarities and differences. Note that the elastic strain energy U_e in the prepeak stage was the ESL. For the similarities, the magnitude of the total energy U_t was the largest, followed by the dissipated energy U_d, and the elastic strain energy U_e was the smallest for all specimens except for the intact coal specimen and the coal specimen containing preformed holes with a 90° relative angle. The reason for this phenomenon may be explained by the failure path of the coal specimens, as plotted in Fig. 7. When the shear plane was shorter, less energy was required, and more energy was stored. The differences between the schemes were the variation tendencies of three types of energy. For schemes one and four, the total energy U_t, elastic strain energy U_e and dissipated energy U_d gradually decreased as the diameter and number of preformed holes increased, respectively. For schemes two and three, the total energy U_t, elastic strain energy U_e and dissipated energy U_d first decreased, then remained approximately constant and finally increased, exhibiting a U-shaped trend. However, the dissipated energy U_d in scheme three did not exhibit this U-shaped trend; the variation trend of the dissipated energy U_d in scheme three was similar to that in schemes one and

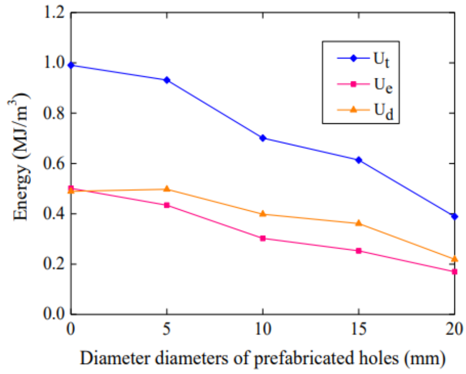

(a) Various diameters of preformed holes

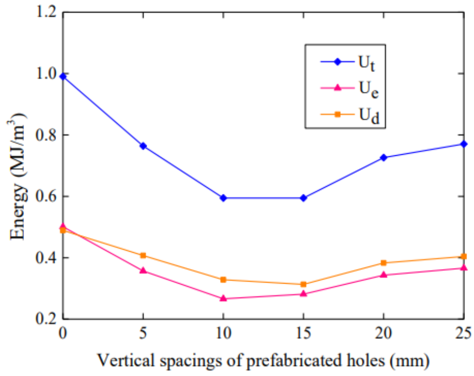

(b) Various vertical spacings of preformed holes

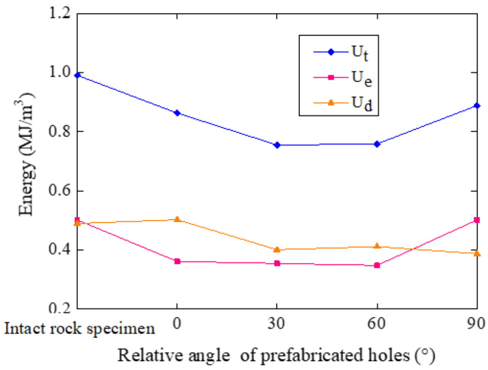

(c) Various relative angles of preformed holes

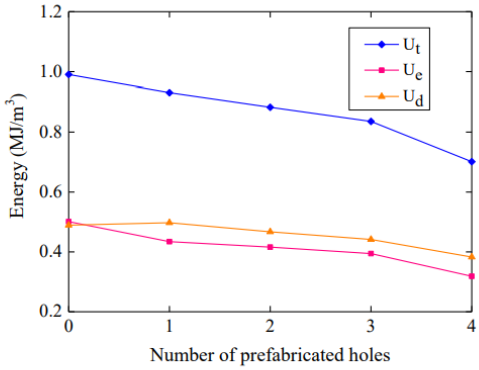

(d) Various numbers of preformed holes

Fig. 9 Energy evolution of coal specimens in the prepeak stage

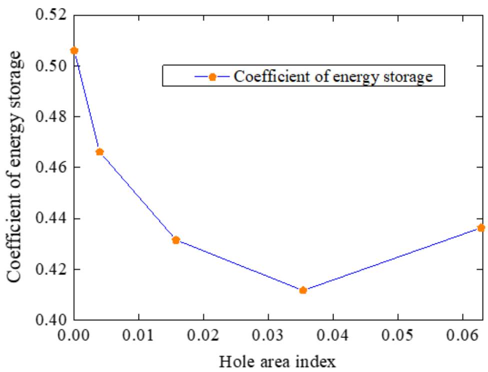

(a) Various area indices of preformed holes

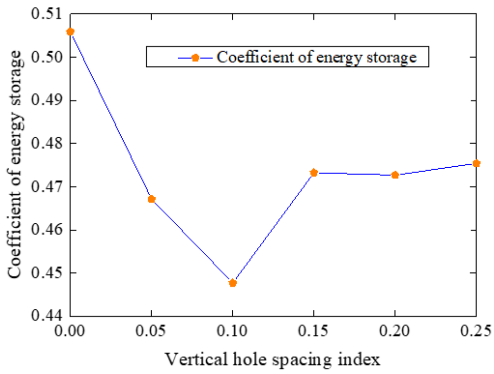

(b) Various vertical spacing indices of preformed holes

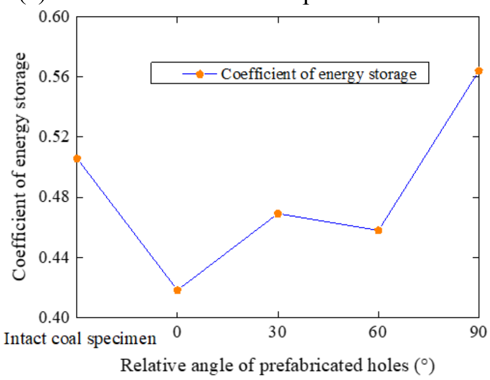

(c) Various relative angles of preformed holes

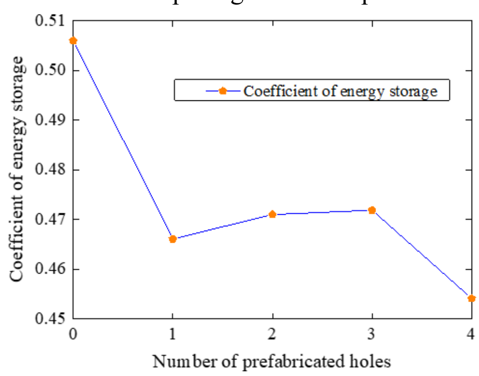

(d) Various numbers of preformed holes

Fig. 10 Elastic energy storage ratio of the coal specimens in the prepeak stage

four. It is worth noting that the variation tendency of the elastic strain energy U_e was more consistent with that of the total energy U_t. Therefore, using a single index of elastic energy or total energy cannot represent the ability of coal specimens to store unstable energy.

4.6 Elastic energy storage ratio in the prepeak stage

To describe the energy conversion of coal specimens under uniaxial compression, the elastic energy storage ratio *m* was investigated. The elastic energy storage ratio *m* was defined as the ratio of elastic strain energy to total energy. When the elastic energy storage ratio *m* is higher, the proportion of stored elastic energy is larger. Correspondingly, the proportion of dissipated energy is small in the coal specimens. A specimen will easily lose its equilibrium and be destroyed when subjected to external disturbances in the critical state. In contrast, the coal specimens in the critical state are not easily disturbed by external disturbances. Therefore, the larger the elastic energy storage ratio *m* is, the stronger the shock of the coal rock at failure. In addition, to better study the effect of the preformed hole diameter and the vertical spacing of two preformed holes, the concept of the preformed hole area index *K* and the preformed hole vertical spacing index *L* were proposed. The ratio of the circular area to the coal specimen area was used to describe the size of the preformed hole area in the unit area of the coal sample. Here, the coal specimen area is referring to the length of the numerical model times its width. Moreover, the ratio of the spacing between the two vertical preformed holes to the height of the coal specimen was used to describe the distribution density of preformed holes in the vertical direction of the coal sample.

Fig. 10 shows the coefficient of energy storage of the coal specimens in the prepeak stage. The results showed that the change trends of the coefficient of energy storage *m* of the coal specimens were different. Fig. 10(a) shows that the coefficient of energy storage *m* of the coal specimens first decreased and then increased as the preformed hole area index *K* increased from 0 (intact coal specimen) to 0.0628. The maximum and minimum values of the elastic energy storage ratio *m* were 50.60% and 41.62% with an area index *K* of 0 and 0.03533, respectively. Fig. 10(b) shows that the elastic energy storage ratio *m* of the intact coal specimen was larger than that of the two preformed holes with various vertical spacing indices *L*. In addition, the elastic energy storage ratio *m* of the coal specimen first decreased, then increased and finally remained approximately constant as the preformed hole vertical spacing index *L* of the preformed hole increased from 0 to 0.25 when the diameter of the preformed hole was 8 mm. The minimum value of the elastic energy storage ratio *m* was 47.28% when the preformed hole vertical spacing index *L* of the preformed hole was 0.1. Fig. 10(c) shows that the elastic energy storage ratio *m* of the intact coal specimen was greater than that of the two preformed holes with various relative angles. Then, the elastic energy storage ratio *m* of the coal specimens first increased, slightly decreased and quickly increased as the relative angles of the preformed holes increased from 0° to 90° at 30° intervals. The maximum and minimum values of the elastic energy storage ratio *m* were 56.41% and 41.82%, respectively, which corresponded to 90° and 0° relative angles of the preformed holes, respectively. Fig. 10(d) shows that the elastic energy storage ratio *m* of the coal specimens first significantly decreased, then slightly increased and finally quickly decreased when the number of preformed holes increased from 0 to 4 at intervals of 1. Therefore, the arrangement of the preformed holes altered the proportion of elastic strain energy U_e in the total energy in the prepeak stage.

5. Discussion

During the entire deformation and failure process of coal, part of the accumulated energy is dissipated to promote the initiation and development of cracks, and the rest of the energy is stored in the coal in the form of elastic strain energy U_e. Once the elastic strain energy U_e exceeds the ESL, this energy will be quickly released in the form of kinetic energy. If the kinetic energy is sufficiently large, the coal fragments will be ejected at a high speed, and a rock burst occurs (Hazzard *et al.* 2000; Fan *et al.* 2016). It is widely accepted that preformed hole distressing could decrease the elastic strain energy U_e in the prepeak stage of coal (Hazzard *et al.* 2000). Although it is not yet possible to determine the thresholds at which rock failure will be prevented, the elastic energy storage ratio *m* can predict the probability of rock failure under certain conditions. Therefore, we can take some measures to reduce the elastic energy storage ratio *m* for weakening the speed of coal fragments.

According to the above results from the numerical simulations, the arrangement of the preformed holes can be reasonably designed for releasing stresss and preventing rock bursts. For better stress release, the diameter, distance and relative angle of preformed holes should be as large as possible, 2*D* (*D* is the hole diameter) and 30° to 90°, respectively. In addition, the number of preformed holes can also be reasonably increased. This paper discussed the diameter selection, vertical spacing selection, relative angle selection and number selection of preformed holes, and provided a technical basis for comprehensive prevention and control of rock bursts, which can be used as a reference for mines with rock burst hazards. Those parameters should be suitably adjusted according to the field conditions to successfully mitigate rock burst hazards.

6. Conclusions

Conventionally, the micro-parameters of the PFC model had been calibrated based on the laboratory test to ensure the reliability of the results. The characteristics of crack initiation stress, cumulative crack number, failure pattern, dissipated energy and elastic strain energy during the loading process were analyzed. A larger single hole diameter would significantly reduce crack initiation stress and promote energy dissipation. Spacing, relative angle and number of preformed holes would affect the size, direction relative to the loading and shape of the rock bridges. Stress is mainly gathering in the rock bridges during loading. The mechanical properties of rock bridges become key factors for energy revolution, formation of energy storage structure, failure property and stress release. To describe the energy conversion in the coal specimens containing preformed holes with various arrangements, the elastic energy storage ratio *m* was investigated. The results showed that the arrangement of the preformed holes altered the energy storage *m* in the prepeak stage, and the probability of rock bursts can be qualitatively discussed.

Acknowledgments

This study is supported by the National Natural Science Foundation of China (Grant No. 51779031 and 41977219).

Conflicts of interest

The author(s) declares no potential conflicts of interest with respect to the research, authorship, and/or publication of this article.

References

Bagde, M.N. and Petroš, V. (2009), "Fatigue and dynamic energy behaviour of rock subjected to cyclical loading", *Int. J. Rock Mech. Min. Sci.*, **46**(1), 200-209. https://doi.org/10.1016/j.ijrmms.2008.05.002.

Bratov, V. and Petrov, Y. (2007), "Optimizing energy input for fracture by analysis of the energy required to initiate dynamic mode I crack growth", *Int. J. Solids Struct.*, **44**(7-8), 2371-2380. https://doi.org/10.1016/j.ijsolstr.2006.07.013.

Bruning, T., Karakus, M., Nguyen, G.D. and Goodchild, D. (2018), "Experimental Study on the Damage Evolution of Brittle Rock Under Triaxial Confinement with Full Circumferential Strain Control", *Rock Mech. Rock Eng.*, **51**(11), 3321-3341. https://doi.org/10.1007/s00603-018-1537-7.

Calleja, J. and Nemcik, J. (2016), "Coalburst Causes and Mechanisms", *Proceedings of the Coal Operators Conference*, Wollongong, Australia, February.

Cho, N., Martin, C.D. and Sego, D.C. (2007), "A clumped particle model for rock", *Int. J. Rock Mech. Min. Sci.*, **44**(7), 997-1010. https://doi.org/10.1016/j.ijrmms.2007.02.002.

Fakhimi, A., Carvalho, F., Ishida, T. and Labuz, J.F. (2002), "Simulation of failure around a circular opening in rock", *Int. J. Rock Mech. Min. Sci.*, **39**(4), 507-515. https://doi.org/10.1016/S1365-1609(02)00041-2.

Fan, L. and Liu, S. (2017), "A conceptual model to characterize and model compaction behavior and permeability evolution of broken rock mass in coal mine gobs", *Int. J. Coal Geol.*, **172**, 60-70. https://doi.org/10.1016/j.coal.2017.01.017.

Fan, L. and Liu, S. (2019), "Fluid-dependent shear slip behaviors of coal fractures and their implications on fracture frictional strength reduction and permeability evolutions", *Int. J. Coal Geol.*, **212**, 103235. https://doi.org/10.1016/j.coal.2019.103235.

Gong, B., Jiang, Y. and Chen, L. (2019) "Feasibility investigation of the mechanical behavior of methane hydrate-bearing specimens using the multiple failure method", *J. Nat. Gas. Sci. Eng.*, 102915. https://doi.org/10.1016/j.jngse.2019.102915.

Hazzard, J.F., Young, R.P. and Maxwell, S.C. (2000), "Micromechanical modeling of cracking and failure in brittle rocks". *J. Geophys. Res. Solid Earth*, **105**(B7), 16683-16697. https://doi.org/10.1029/2000jb900085.

Hebblewhite, B. and Galvin, J. (2017), "A review of the geomechanics aspects of a double fatality coal burst at Austar Colliery in NSW, Australia in April 2014", *Int. J. Min. Sci. Technol.*, **27**(1), 3-7. https://doi.org/10.1016/j.ijmst.2016.10.002.

Huang, Y.H., Yang, S.Q. and Tian, W.L. (2019), "Cracking process of a granite specimen that contains multiple pre-existing holes under uniaxial compression", *Fatigue Fract. Eng. Mater. Struct.*, **42**(6), 1341-1356. https://doi.org/10.1111/ffe.12990.

Jin, P.J., Wang, E.Y. and Song, D.Z. (2017), "Study on correlation of acoustic emission and plastic strain based on coal-rock damage theory" *Geomech. Eng.*, **12**(4), 627-637. https://doi.org/10.12989/gae.2017.12.4.627.

José, A., Sanchidrián, P.S. and López, L.M. (2007), "Energy components in rock blasting", *Int. J. Rock Mech. Min. Sci.*, **44**(1), 130-147. https://doi.org/10.1016/j.ijrmms.2006.05.002.

Kim, J.S., Kim, G.Y., Baik, M.H., Finsterle, S. and Cho, G.C. (2019), "A new approach for quantitative damage assessment of in-situ rock mass by acoustic emission", *Geomech. Eng.*, **18**(1), 11-20. https://doi.org/10.12989/gae.2019.18.1.011.

Li, Y.H., Peng, J.Y., Zhang, F.P. and Qiu, Z.G. (2016) "Cracking behavior and mechanism of sandstone containing a pre-cut hole under combined static and dynamic loading", *Eng. Geol.*, **213**(4), 64-73. https://doi.org/10.1016/j.enggeo.2016.08.006.

Lin, P., Wong, R.H.C. and Tang, C.A. (2015), "Experimental study of coalescence mechanisms and failure under uniaxial compression of granite containing multiple holes", *Int. J. Rock Mech. Min. Sci.*, **77**, 313-327. https://doi.org/10.1016/j.ijrmms.2015.04.017.

Marek, U. (2009), "Monitoring of methane and rockburst hazards as a condition of safe coal exploitation in the mines of Kompania Weglowa SA", *Proc. Earth Planet. Sci.*, **1**(1), 54-59. https://doi.org/10.1016/j.proeps.2009.09.011.

Mark, C. (2016), "Coal bursts in the deep longwall mines of the United States", *Int. J. Coal Sci. Technol.*, **3**(1), 1-9. https://doi.org/10.1007/s40789-016-0102-9.

Mark, C. and Gauna, M. (2016), "Evaluating the risk of coal bursts in underground coal mines", *Int. J. Min. Sci. Technol.*, **26**(1), 47-52. https://doi.org/10.1016/j.ijmst.2015.11.009.

Mu, W., Li, L., Yang, T., Yu, G. and Han, Y. (2019), "Numerical investigation on a grouting mechanism with slurry-rock coupling and shear displacement in a single rough fracture", *Bull. Eng. Geol. Environ.*, **4**, 1-19. https://doi.org/10.1007/s10064-019-01535-w.

Munoz, H., Taheri, A. and Chanda, E.K. (2016), "Rock drilling performance evaluation by an energy dissipation based rock brittleness index", *Rock Mech. Rock Eng.*, **49**(8), 3343-3355. https://doi.org/10.1007/s00603-016-0986-0.

Nugroho A. and Purnama A.B. (2015), "Displacement distribution model of andesite rock mass due to blasting activity using finite element method", *Indo. Min. J.*, **18**(2), 47-58. https://doi.org/10.30556/imj.Vol18.No2.2015.289.

Park J.W., Park D., Ryu D.W., Choi B.H. and Park E.S. (2014), "Analysis on heat transfer and heat loss characteristics of rock cavern thermal energy storage", *Eng. Geol.*, **181**, 142-156. https://doi.org/10.1016/j.enggeo.2014.07.006.

Potyondy, D.O. and Cundall, P.A. (2004), "A bonded-particle model for rock", *Int. J. Rock Mech. Min. Sci.*, **41**(8), 1329-1364. https://doi.org/10.1016/j.ijrmms.2004.09.011.

Sagasta, F., Zitto, M.E., Piotrkowski, R., Benavent-Climent, A., Suarez, E. and Gallego, A. (2018), "Acoustic emission energy b-value for local damage evaluation in reinforced concrete structures subjected to seismic loadings", *Mech. Syst. Signal Proc.*, **102**, 262-277. https://doi.org/10.1016/j.ymssp.2017.09.022.

Sarfarazi, V., Haeri, H., Shemirani, A.B. and Nezamabadi, M.F. (2018), "A fracture mechanics simulation of the pre-holed concrete Brazilian discs", *Struct. Eng. Mech.*, **66**(3), 343-351.

https://doi.org/10.12989/sem.2018.66.3.343.
Singh, S.P. (1988), "Burst energy release index", *Rock Mech. Rock Eng.*, **21**(2), 149-155. https://doi.org/10.1007/BF01043119.
Steffler, E.D., Epstein, J.S., and Conley, E.G. (2003), "Energy partitioning for a crack under remote shear and compression", *Int. J. Fract.*, **120**(4), 563-580. https://doi.org/10.1023/A:1025511703698.
Sujatha, V. and Kishen, J.C. (2003), "Energy release rate due to friction at bimaterial interface in dams", *J. Eng. Mech.*, **129**(7), 793-800. https://doi.org/10.1061/(asce)0733-9399(2003)129:7(793).
Wang, J., Ning, J.G, Qiu, P.Q., Yang, S. and Shang, H.F. (2019), "Microseismic monitoring and its precursory parameter of hard roof collapse in longwall faces: A case study", *Geomech. Eng.*, **17**(4), 375-383. https://doi.org/10.12989/gae.2019.17.4.375.
Wasantha, P.L.P., Ranjith, P.G. and Shao, S.S. (2014), "Energy monitoring and analysis during deformation of bedded-sandstone: Use of acoustic emission", *Ultrasonics*, **54**(1), 217-226. https://doi.org/10.1016/j.ultras.2013.06.015.
Wong, R.H.C., Lin, P., and Tang, C.A. (2006), "Experimental and numerical study on splitting failure of brittle solids containing single pore under uniaxial compression", *Mech. Mater.*, **38**(1-2), 142-159. https://doi.org/10.1016/j.mechmat.2005.05.017.
Zhang, M.S., Wang, S.H., and Yang, Y. (2011), "Numerical simulation of jointed rock mass constitutive model and its validation", *Eng. Mech.*, **28**(5), 26-30. https://doi.org/10.1631/jzus.A1000257.
Zitto, M.E., Piotrkowski, R., Gallego, A., Sagasta, F. and Benavent-Climent A. (2015), "Damage assessed by wavelet scale bands and b-value in dynamical tests of a reinforced concrete slab monitored with acoustic emission", *Mech. Syst. Signal Proc.*, **60**, 75-89. https://doi.org/10.1016/j.ymssp.2015.02.006.

CC